Applied Catalysis B: Environmental 84 (2008) 420–425

Contents lists available at ScienceDirect

Applied Catalysis B: Environmental

journal homepage: www.elsevier.com/locate/apcatb

Formation of active sites on $Ir/WO_3–SiO_2$ for selective catalytic reduction of NO by CO

Tetsuya Nanba *, Satoru Shinohara, Shouichi Masukawa, Junko Uchisawa, Akihiko Ohi, Akira Obuchi

National Institute of Advanced Industrial Science and Technology (AIST), Research Center for New Fuels and Vehicle Technology, 16-1 Onogawa, Tsukuba 305-8569, Japan

ARTICLE INFO

Article history:
Received 10 January 2008
Received in revised form 18 April 2008
Accepted 22 April 2008
Available online 8 May 2008

Keywords:
Nitrogen oxide
Carbon monoxide
Iridium
Selective catalytic reduction
Tungsten oxide
Silica

ABSTRACT

Pretreatment conditions for the activation of $Ir/WO_3–SiO_2$ for the selective catalytic reduction of NO by CO in the presence of excess O_2 were studied. Sequential treatment involving calcination in the presence of O_2 and H_2O followed by reduction and then re-oxidation under mild conditions was found to effectively activate $Ir/WO_3–SiO_2$. Temperature-programmed desorption during calcination, X-ray diffraction, and temperature-programmed reduction by H_2 revealed that calcination was necessary for oxidative removal of the NH_3 ligands from the iridium precursor, that reduction produced metallic iridium and partially reduced tungsten oxide, and that re-oxidation produced tungsten oxide with low reducibility. Transmission electron microscopy revealed that Ir was supported on finely dispersed tungsten oxide and that the iridium particle size after the sequential activation was 1–1.5 nm.

1. Introduction

Selective catalytic reduction (SCR) of NO_x ($NO + NO_2$) by reductants present in exhaust gases is an attractive way to control NO_x emissions from diesel and lean-burn engines. Since Iwamoto et al. [1] and Held et al. [2] discovered SCR by hydrocarbons (HC-SCR), many papers on HC-SCR have been published [3]. Many kinds of catalysts, such as platinum-group metals [4,5], zeolites [6,7], and Al_2O_3-supported transition metals [8,9], exhibit HC-SCR activity. However, no HC-SCR catalytic converter system is yet in practical use.

A new type of internal combustion engine is being developed for the reduction of NO_x emissions: the homogeneous charge compression ignition (HCCI) engine. This engine shows low NO_x and particulate emissions and relatively high-CO emissions [10]. Therefore, the use of CO as a reductant for exhausts with low-NO_x concentrations is of interest. Although CO acts as a reductant in the three-way catalyst [11], it is a poor reductant under lean conditions [12,13]. Recently, iridium catalysts have been reported to show CO-SCR activity. For example, Ogura et al. reported that Ir/silicalite at a very low-Ir loading exhibits high activity in the absence and presence of SO_2 [14]. Haneda et al. reported that Ir/SiO_2 shows high activity only in the presence of SO_2 [15]. Shimokawabe et al. reported that Ir/WO_3 and Ir/ZnO show high activities [16] and that Ir/WO_3 is effective even in the presence of SO_2 [17]. Because the sulfur content in diesel fuel is now severely restricted in many countries, a catalyst having CO-SCR activity in the absence of SO_2 is desirable. We have recently found that the combination of WO_3 and SiO_2 is an effective catalyst support [18]. The $Ir/WO_3–SiO_2$ is composed of Ir/WO_3 highly dispersed on SiO_2. In this study, we attempted to optimize the preparation conditions for the formation of active sites during preparation of the supported catalyst, and we discuss the active state of the Ir/WO_3.

2. Experimental

2.1. Catalyst preparation

The combined oxide support, $WO_3–SiO_2$, was prepared by two methods. *Method 1*. Addition of metallic tungsten powder (Mitsuwa Chemical Co.) to 15% H_2O_2 yielded a peroxopolytungstic acid solution [19]. After the pH of this solution was adjusted to approximately 8.5 with NH_3, a predetermined amount of silica sol was added (Cataloid S-20L, containing 20 wt% SiO_2; Catalysis & Chemical IND Co.). The mixture was dried at 110 °C and calcined in air at 500 °C for 4 h. *Method 2*. Ammonium tungstate *para*-pentahydrate (Wako Pure Chemical Industries) [$(NH_4)_{10}W_{12}O_{41}\cdot 5H_2O$], was dissolved in 0.7 M malic acid aqueous solution. A predetermined amount of silica sol was added, and the pH was adjusted to approximately 8.8 with NH_3. Gelation occurred within

* Corresponding author. Tel.: +81 29 861 8288; fax: +81 29 861 8259.
E-mail address: tty-namba@aist.go.jp (T. Nanba).

0926-3373/$ – see front matter © 2008 Elsevier B.V. All rights reserved.
doi:10.1016/j.apcatb.2008.04.027

1 h after the addition of NH_3. The gel was dried at 100 °C and calcined in air at 500 °C for 4 h. The WO_3–SiO_2 made by method 1 was prepared with WO_3 contents ranging from 0% to 100%. The mixed oxide support is designated $WO_3(x)$–SiO_2-1 or -2, where the value in parentheses is the weight percentage of WO_3 in the support and the next number is the preparation method.

Iridium supported on WO_3–SiO_2 was prepared by the impregnation method using $Ir(NH_3)_6(OH)_3$ as a precursor. The loading of iridium was adjusted from 0.25 to 10 wt%. The impregnated supports were calcined at 500 °C for 4 h under various atmospheres.

2.2. Activity tests

Catalytic activity tests were conducted in a conventional fixed-bed reactor at atmospheric pressure. The catalyst (0.1 g; sieved to between 0.15 and 0.25 mm) was diluted with quartz sand or SiC granules (particle size, 0.3–0.5 mm). The flow rate of the feed gas was 225 or 400 mL/min, corresponding to a space velocity of 34,000 or 60,000 h^{-1}, respectively. The feed gas composition for the 225 mL/min flow rate was 500 ppm NO, 5000 ppm CO, 10% O_2, and 1% H_2O, with He as a balance gas; for the 400 mL/min flow rate, the feed gas composition was 500 ppm NO, 3000 or 5000 ppm CO, 10% O_2, and 1% or 6% H_2O, with N_2 as a balance gas. Before most of the catalytic activity tests, the catalysts were reduced in 10% H_2 at 600 °C for 1 h. The temperature dependence of the catalytic activity was measured from 400 to 180 °C in steps of 10 °C. At each temperature, the effluent gas was sampled after the temperature had been maintained for 1 h. In the other activity test, in which measurements were carried out at a constant temperature of 270 °C, the samples were pretreated under various conditions after the H_2 reduction. Concentrations of NO, NO_2, N_2O, CO, and CO_2 in the reactant and product gases were analyzed with an FT-IR spectrometer (Magna 560; Nicolet) equipped with a multi-reflectance gas cell (Gemini Specialty Optics, optical path length, 2 m) and a mercury–cadmium–telluride detector. For the feed gas balanced with He, a gas chromatograph (M200; Agilent) equipped with an MS-5A PLOT column (for N_2 and CO) or a PoraPLOT Q column (for CO_2 and N_2O) and a thermal conductivity detector was also used. The catalytic activity was evaluated in terms of NO_x conversion and N_2 selectivity. To ensure accuracy, N_2 selectivity was evaluated only when the NO_x conversion was above 10%:

$$NO_x \text{ conversion} = \frac{[\text{inlet } NO_x] - [\text{outlet } NO_x]}{[\text{inlet } NO_x]} \times 100$$

$$N_2 \text{ selectivity (for He balance)} = \frac{[\text{outlet } N_2]}{[\text{outlet } N_2] + [\text{outlet } N_2O]} \times 100$$

$$N_2 \text{ selectivity (for } N_2 \text{ balance)} = \left\{1 - 2 \times \left[\frac{[\text{outlet } N_2O]}{[\text{inlet } NO_x] - [\text{outlet } NO_x]}\right]\right\} \times 100$$

2.3. Characterization

The Brunauer–Emmett–Teller (BET) specific surface area was measured by N_2 adsorption under a flow condition (Model 4232; Nikkiso). X-ray diffraction (XRD) patterns were measured at 40 kV and 100 mA of X-ray power (RU-300; Rigaku). Identification of crystal phase was carried out by using the JCPDS database. Temperature-programmed reduction by H_2 (H_2-TPR) was carried out in an adsorption test apparatus equipped with a thermal conductivity detector (ADT700; Ohkura-Riken). The TPR profiles were obtained from room temperature to 600 °C in a 100 mL/min flow of 2% H_2/Ar at a heating rate of 10 °C/min after oxidation of the sample in a 5% O_2 flow at 500 °C for 2 h. The morphologies of Ir and WO_3 particles were observed by transmission electron microscopy (TEM; JEM2000EX; JEOL). Temperature-programmed desorption (TPD) of nitrogen-containing compounds was carried out to clarify how the Ir precursor decomposed during these calcination procedures. After Ir loading and drying, 0.1 g of the sample was placed in the apparatus used for the activity tests. The TPD profiles were obtained from room temperature to 500 °C in a 100 mL/min flow of 10% H_2, 20% O_2, or 20% O_2 + 1% H_2O at a heating rate of 5 °C/min.

3. Results

3.1. Catalytic activity

Table 1 lists the CO-SCR activities of 0.5 wt% Ir/WO_3–SiO_2-1 with various WO_3 contents. At WO_3 contents above 50%, the maximum NO_x conversion and N_2 selectivity at the temperature of maximum NO_x conversion were almost the same as those of Ir/WO_3. At WO_3 contents below 30%, the activity was markedly enhanced. Note that a high activity was attained even at 1 wt% WO_3. WO_3 contents of 1–30 wt% correspond to W/Ir molar ratios between 1.7 and 50. Note also that the precursor of WO_3 had a negligible influence on the CO-SCR activity. We confirmed that the crystal phases of the WO_3 in the Ir/WO_3–SiO_2-1 and -2 samples were the same, monoclinic and orthorhombic. The fact that the two samples were composed of the same crystal phases indicates that the WO_3 precursor probably had no influence on the crystal phase.

Examination of the activities at various Ir loadings showed that the maximum NO_x conversion was achieved at 0.5 wt% (Table 2), and CO conversion increased with increasing Ir loading. N_2 selectivity decreased with increasing Ir loading.

3.2. Effect of calcination, reduction, and additional pretreatment conditions

We investigated the effects of calcination conditions on the activity of 0.5 wt% Ir/WO_3(10)–SiO_2-2 in terms of the maximum

Table 1
Effect of WO_3 content on CO-SCR activity

WO_3 content (wt%)	Temperature (°C)	NO_x conversion (%)	N_2 selectivity (%)
0	250	11	81
1	260	85	89
10	260	86	89
30	265	82	87
40	265	69	81
50	255	49	79
80	275	42	72
100	270	39	79

Catalyst: 0.5 wt% Ir/$WO_3(x)$–SiO_2-1; catalyst weight: 0.1 g; flow rate: 225 mL/min; composition: 500 ppm NO, 5000 ppm CO, 10% O_2, 1% H_2O, and balance He.

Table 2
Effect of iridium loading on CO-SCR activity

Loading (wt%)	NO_x conversion (%)[a]	CO conversion (%)	N_2 selectivity (%)
0.25	21	37	68
0.5	34	51	68
1	25	79	58
2	22	91	51
5	21	91	45
10	18	95	41

Catalyst: 0.5 wt% Ir/WO_3(10)–SiO_2-2; catalyst weight: 0.1 g; flow rate: 400 mL/min; composition: 500 ppm NO, 3000 ppm CO, 10% O_2, 6% H_2O, and balance N_2.
[a] Maximum NO_x conversion. CO conversion and N_2 selectivity were measured at 280 °C.

Table 3
Effect of calcination condition on CO-SCR activity

Calcination condition	Reaction temperature (°C)	NO_x conversion (%)	CO conversion (%)	N_2 selectivity (%)
Air, 500 °C	275	34	51	68
20% O_2, 500 °C	260	7	81	–
20% O_2 + 1% H_2O, 500 °C	280	26	66	65
1% O_2 + 6% H_2O, 500 °C	275	31	72	68
6% H_2O, 500 °C	330	10	98	48
10% H_2, 600 °C[a]	290	4	97	–

Catalyst: 0.5 wt% Ir/WO_3(10)–SiO_2-2; catalyst weight: 0.1 g; flow rate: 400 mL/min; composition: 500 ppm NO, 3000 ppm CO, 10% O_2, 6% H_2O, and balance N_2. After calcination, sample was reduced in H_2 at 600 °C for 1 h, and then activity was measured as the manner of temperature dependence.
[a] Reduction procedure as pretreatment was omitted.

Table 4
Effect of reduction condition on CO-SCR activity

Reduction condition	NO_x conversion (%)	CO conversion (%)	N_2 selectivity (%)
10% H_2, 600 °C[a]	81	82	88
Non[a]	33	66	72
10% H_2, 400 °C[b]	26	61	62
10% H_2, 500 °C[b]	29	71	64
10% H_2, 600 °C[b]	31	72	68

Catalyst: 0.5 wt% Ir/WO_3(10)–SiO_2-1; catalyst weight: 0.1 g; calcination condition was in air at 500 °C for 4 h. Activity was measured as the manner of temperature dependence.
[a] Flow rate: 225 mL/min; composition: 500 ppm NO, 5000 ppm CO, 10% O_2, 1% H_2O, and balance He. Reaction temperature was 270 °C.
[b] Flow rate: 400 mL/min; composition: 500 ppm NO, 3000 ppm CO, 10% O_2, 6% H_2O, and balance N_2. Reaction temperature was 280 °C.

NO_x conversion as well as the CO conversion and N_2 selectivity at the temperature of maximum NO_x conversion (Table 3). Among the catalysts calcined in various atmospheres, the catalysts calcined in ambient air showed the highest NO_x conversion. The catalyst calcined in 20% O_2 showed very low activity, whereas the catalyst calcined in 20% O_2 + 1% H_2O showed higher activity. Furthermore, the catalyst calcined in 1% O_2 + 6% H_2O showed activity comparable to that of the catalyst calcined in air, whereas the catalyst calcined in 6% H_2O showed low activity. The catalyst calcined in 10% H_2 also showed low activity. The catalysts showing low-NO_x conversions exhibited relatively high-CO conversions. These results suggest that the co-existence of O_2 and H_2O was necessary for activation of the catalyst.

We compared the activities of reduced and unreduced catalysts after calcination and found that the reduced catalysts showed markedly higher NO_x conversion than the unreduced catalysts (Table 4). The maximum NO_x conversions over the catalysts reduced at 400, 500, and 600 °C were 26%, 29%, and 31%, respectively, which suggests that the reduction temperature had little effect on the activity.

We investigated the effects of additional treatment conditions on the activity of 0.5 wt% Ir/WO_3(10)–SiO_2-2, which had been calcined in air and then reduced at 600 °C (Table 5). The catalytic activity was evaluated at 270 °C. When the catalysts were cooled from 400 to 270 °C under a flow of CO-SCR feed gas, the catalysts showed high-NO_x conversions. In contrast, cooling the catalysts under a flow of He resulted in only 7% NO_x conversion. However, the catalysts subjected to additional treatment at 400 °C in 10% O_2 showed approximately 50% NO_x conversion. This result suggests that re-oxidation after reduction effectively activated the catalysts. However, the catalyst pretreated at 600 °C in 100% O_2 was almost inactive, suggesting that mild re-oxidation was better for activation than severe re-oxidation.

3.3. Characteristics of Ir/WO_3–SiO_2

The specific surface area of Ir/SiO_2 was 190 m^2/g, and the value decreased as the WO_3 content increased (Fig. 1). For the samples with 10–80 wt% WO_3, the specific surface area decreased linearly with increasing WO_3. The specific surface area in the range of 80–100 wt% WO_3 also linearly decreased with increasing WO_3. Note that the molar amounts of WO_3 and SiO_2 are almost equivalent at 80 wt% WO_3. The dashed line in Fig. 1 indicates the surface area of SiO_2 contained in 1 g of each Ir/WO_3–SiO_2 catalyst. In the range from 10 to 80 wt% WO_3, the slope of the curve for the SiO_2 surface area is the same as the slope of the curve for the catalysts. These results suggest that the change in specific surface area in this region depended only on the SiO_2 content.

We measured XRD profiles of 0.5 wt% Ir/WO_3(10)–SiO_2-2 after calcination in air, after reduction at 600 °C, and after the CO-SCR activity test (Fig. 2). The sample calcined in air showed peaks due to WO_3 (JCPDS: 43-1035, 20-1324) (Fig. 2(a)), which suggests that WO_3 over SiO_2 was crystalline even at 10 wt% WO_3. For the sample reduced at 600 °C, the WO_3 diffraction peaks disappeared, and peaks ascribed to WO_{3-x} ($0 < x < 1$) (JCPDS: 30-1387), WO_2 (JCPDS: 32-1393), and W metal (JCPDS: 04-0806) were observed (Fig. 2(b)). For the sample subjected to CO-SCR, the XRD profile exhibited broad peaks in the WO_3 region, and the WO_2 and W metal peaks diminished (Fig. 2(c)). The presence of the broad peaks in the WO_3 region (broader than those in Fig. 2(a)) suggests that fine WO_3 particles were formed. In contrast, the sample subjected to severe oxidation conditions (100% O_2 at 600 °C) showed a sharp peak at 23.1° (Fig. 2(d)), which is attributed to WO_3; this treatment did not restore the peak intensity to the original level (Fig. 2(a)).

Table 5
Effect of treatment condition after reduction on CO-SCR activity

Condition	Atmosphere before reaction	NO_x conversion (%)	CO conversion (%)	N_2 selectivity (%)
CO-SCR feed (introduced at 400 °C)	CO-SCR feed[a]	84	84	87
Non	He	7	97	–
CO-SCR feed (400 °C, 1 h)	He	49	73	72
10% O_2 (400 °C, 1 h)	He	54	97	74
100% O_2 (600 °C, 1 h)	He	2	3	–

Activity measurement was carried out at 270 °C. Catalyst: 0.5 wt% Ir/WO_3(10)–SiO_2-2; catalyst weight: 0.1 g; flow rate: 225 mL/min; composition of CO-SCR feed gas: 500 ppm NO, 5000 ppm CO, 10% O_2, 1% H_2O, and balance He. Calcination: 500 °C for 4 h in air; reduction: 600 °C for 1 h in 10% H_2.
[a] Temperature dependence procedure as shown in Fig. 1(a).

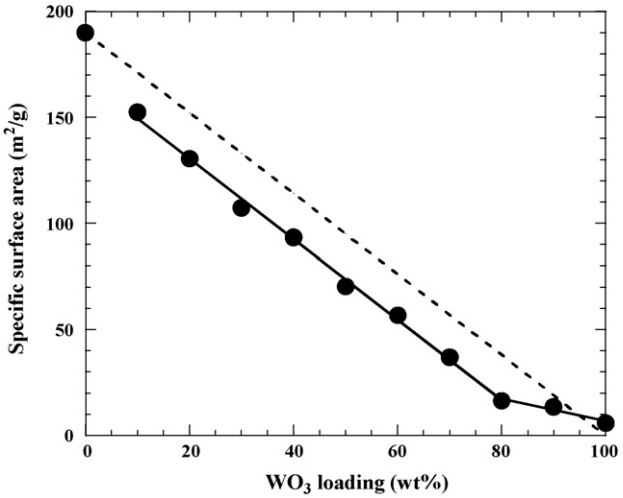

Fig. 1. Dependence of BET surface area on WO_3 content for 0.5 wt% Ir/WO_3(x)–SiO_2-1.

Although crystallization of WO_3 seemed to be promoted by the severe oxidation conditions, the WO_3 particles obtained after calcination, reduction, and severe re-oxidation must have been smaller than those obtained after calcination alone.

We also examined the H_2-TPR profiles for various 0.5 wt% Ir catalysts (Fig. 3). Ir/SiO_2 exhibited a reduction peak at 225 °C, which was assigned to the reduction of IrO_2 to Ir metal. Ir/WO_3 had a broad peak centered at 440 °C, in addition to a peak at 220 °C, whereas WO_3 had no peak below 550 °C. The reduction temperature of WO_3 is known to be lowered in the presence of a noble metal [20,21]. Therefore, we ascribed the broad peak at around 440 °C to the reduction of WO_3. H_2 consumption values for the peaks at around 220 °C for Ir/SiO_2 and Ir/WO_3 were 42 and 310 μmol/g, respectively. These values correspond, respectively, to 0.8 and 6 times the calculated H_2 consumption for stoichiometric reduction of IrO_2 to Ir. The high-H_2 consumption (substantially exceeding unity) suggests that IrO_2 reduction over WO_3 proceeded together with reduction of WO_3. Ir/WO_3(10)–SiO_2-2 exhibited H_2 reduction peaks at 225 and 350 °C. The amount of H_2 consumed below 500 °C corresponded to the formation of $WO_{2.9}$. Additional H_2 was consumed above 550 °C, which suggests that tungsten oxides were reduced further at high temperatures. Re-oxidized Ir/WO_3(10)–SiO_2-2 exhibited a H_2 reduction peak at 190 °C, which we ascribed to the reduction of IrO_2 and WO_3; no other peak appeared below 550 °C, which suggests that the reduction of tungsten oxides was suppressed after the re-oxidization.

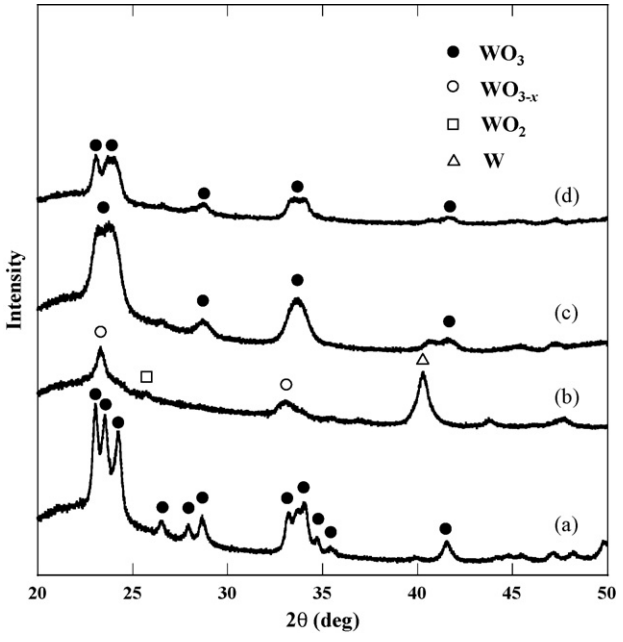

Fig. 2. XRD profiles of 0.5 wt% Ir/WO_3(10)–SiO_2-2 treated under various conditions: (a) after calcination in air, (b) after reduction at 600 °C, (c) after re-oxidation under CO-SCR conditions, and (d) after re-oxidation at 600 °C in 100% O_2.

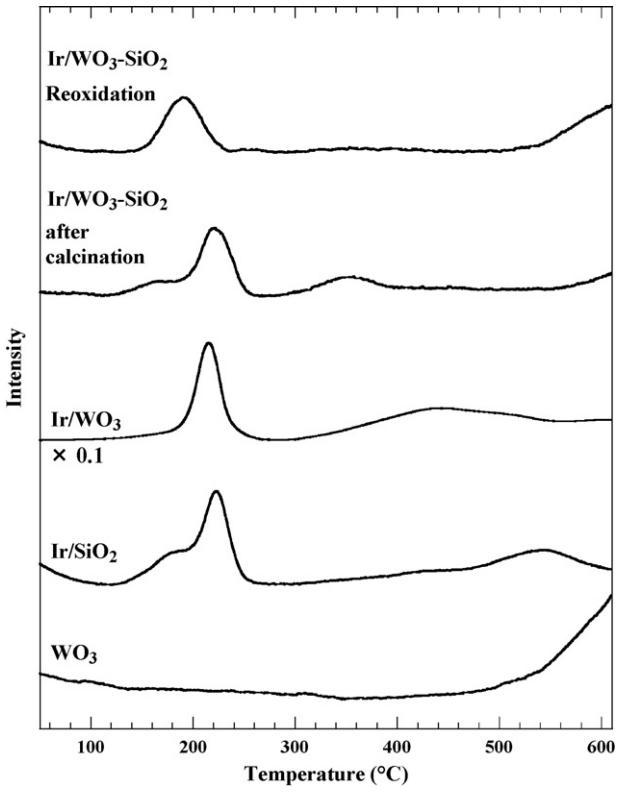

Fig. 3. H_2-TPR profiles of various 0.5 wt% Ir catalysts.

We investigated the H_2-TPR profiles of Ir/WO_3–SiO_2 catalysts with various WO_3 contents (Fig. 4(a)). At WO_3 contents below 10 wt%, the TPR profiles showed a peak at 235 °C with a shoulder at 200 °C. At WO_3 contents above 10 wt%, the shoulder at 200 °C increased and shifted toward lower temperatures as the WO_3 content increased. We determined the molar ratio of H_2 consumed to Ir atoms for the peak at around 220 °C, including the shoulder (or peak) at around 200 °C, and examined the correlation between this ratio and the WO_3 content in 0.5 wt% Ir/WO_3–SiO_2-1 after calcination (Fig. 4(b)). A ratio of 2 suggests stoichiometric reduction of IrO_2 to Ir. Below 30 wt% WO_3, the ratio was slightly lower than 2 at 30 wt% WO_3, the ratio was slightly higher than 2, and as the WO_3 content increased, the ratio increased markedly and substantially exceeded 2. This observed behavior for the peak and the shoulder at $>$ 30 wt% WO_3 indicates that the reducibility of WO_3 in the vicinity of IrO_2 was higher for catalysts containing $>$30 wt% WO_3 than for catalysts containing less WO_3. Lucas et al. reported that the reducibility of WO_3 decreases with decreasing WO_3 content [22]. These results suggest that reduction of WO_3 in the vicinity of IrO_2 did not occur to a substantial extent for catalysts with WO_3 contents below 30 wt% and that the reduction of WO_3 increased with increasing WO_3 content at values above 30 wt%.

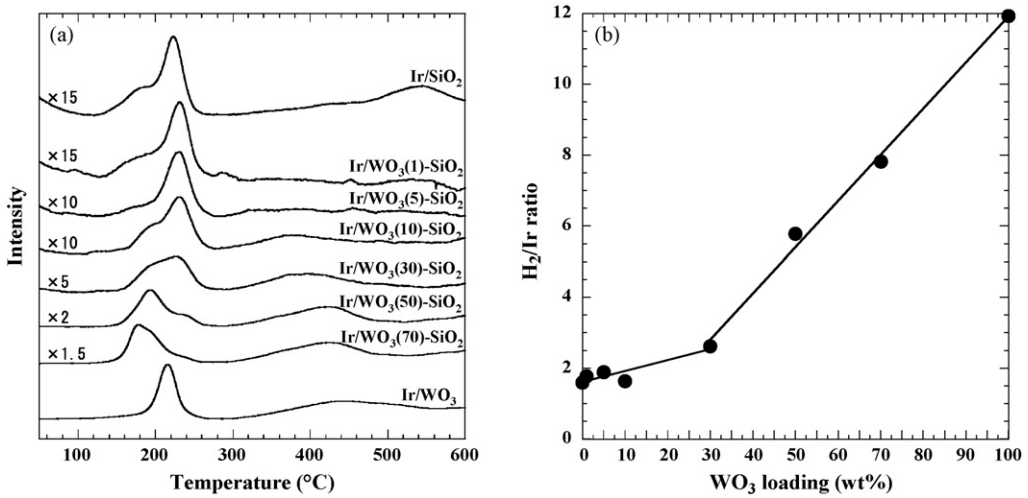

Fig. 4. H_2-TPR profiles of the Ir/WO_3–SiO_2-1 (a) and the molar ratio of H_2 consumed to Ir atoms for the peak at 220 °C and the dependence of the ratio on WO_3 content (b).

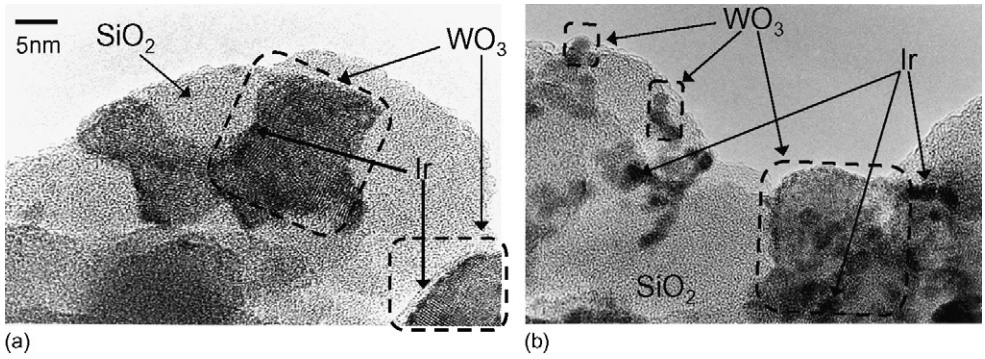

Fig. 5. TEM image of 0.5 wt% Ir/WO_3(10)–SiO_2-2 treated by optimal sequential treatment (a) and reduced without calcination (b).

TEM images of 0.5 wt% Ir/WO_3(10)–SiO_2-2 subjected to CO-SCR conditions showed that cubic tungsten oxides with particle sizes larger than 5 nm were dispersed on SiO_2 and that Ir particles 1–1.5 nm in size were located on the tungsten oxides (Fig. 5(a)). In contrast, TEM images of the reduced 0.5 wt% Ir/WO_3(10)–SiO_2-2 without calcination, which had low activity, exhibited WO_3 particles of various sizes and Ir particles 2–5 nm in size (Fig. 5(b)). Furthermore, there were some Ir particles that were not associated with WO_3 particles, as indicated by the absence of a lattice pattern of WO_3 around the Ir particles. We concluded that the final active form of Ir/WO_3–SiO_2 obtained by sequential treatment involving calcination, reduction, and re-oxidation was very fine Ir/WO_3 particles dispersed on SiO_2.

4. Discussion

The preferred composition of Ir/WO_3–SiO_2 for CO-SCR was 1–30 wt% WO_3 in the support and a 0.5 wt% Ir loading. The surface area of Ir/WO_3–SiO_2 was linearly correlated with SiO_2 content. In contrast, almost equivalent activities of the samples with 1–30 wt% WO_3 loading were observed. Previously, we reported that iridium particles existed selectively on the WO_3 particles, and we supposed that the increase in the surface area of Ir/WO_3 by dispersion on the SiO_2 resulted in the enhancement of the CO-SCR activity [18]. However, these results suggest that the enhancement of the CO-SCR activity of Ir/WO_3–SiO_2 at lower WO_3 contents was due not to an increase in the Ir/WO_3 surface area but to some other reason, which is discussed below.

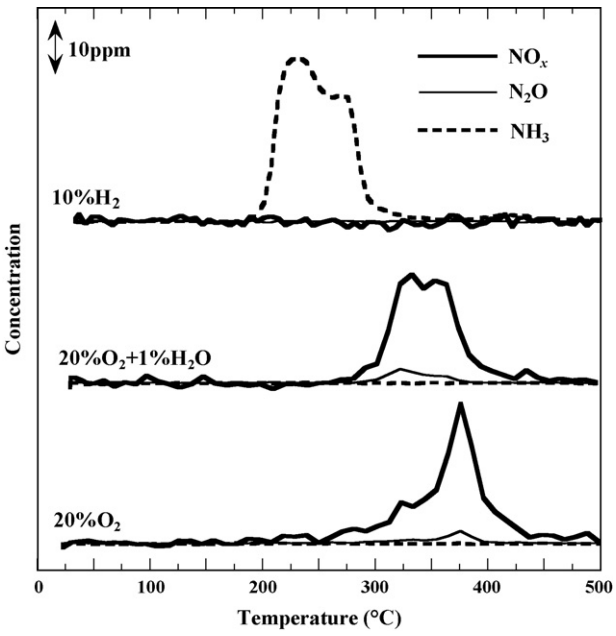

Fig. 6. Temperature-programmed desorption of nitrogen-containing compounds during calcination under 10% H_2, 20% O_2, and 20% O_2 + 1% H_2O. Catalyst weight, 0.1 g; flow rate, 400 mL/min; ramping rate, 5 °C/min.

The change in CO-SCR activity with WO_3 content agreed well with the change in the reduction properties of IrO_2 and WO_3 at 220 °C as revealed by H_2-TPR (Fig. 4). This result suggests that what makes WO_3 preferable as a support for Ir is its resistance to reduction when in the vicinity of Ir particles.

To activate $Ir/WO_3–SiO_2$, the catalysts had to be treated sequentially by calcination (oxidation in the presence of H_2O), reduction, and re-oxidation. TEM observations indicated that the reduced sample without calcination had larger Ir particles than the sample subjected to the optimal sequential treatment and that the former sample had separate Ir and WO_3 particles. Ir/SiO_2 is known to exhibit activity only in the presence of SO_2 [15], so the decrease in the CO-SCR activity of the reduced catalysts without calcination was probably due to dissociation of Ir from WO_3. To observe the decomposition behavior of Ir precursor, we used TPD to measure the formation of nitrogen-containing compounds from $WO_3–SiO_2$ impregnated with $Ir(NH_3)_6(OH)_3$ (Fig. 6). NO_x and N_2O formed at 375 °C in 20% O_2. Furthermore, the addition of H_2O to 20% O_2/N_2 led to the evolution of NO_x at a lower temperature of approximately 335 °C. This result suggests that calcination in the presence of O_2 and H_2O resulted in the H_2O-promoted oxidative removal of ligands of $Ir(NH_3)_6(OH)_3$. On the other hand, calcination under H_2/N_2 resulted in NH_3 formation between 200 and 300 °C, which suggests the simple release of NH_3 ligands. Considering that H_2 reduction after calcination was performed in the absence of NH_3 ligands for the active $Ir/WO_3–SiO_2$, the residual NH_3 ligands might relate to the dissociation of Ir form WO_3 in the reducing conditions. The role of calcination is suspected to be the oxidative removal of NH_3 ligands.

H_2 reduction after calcination was necessary for activating $Ir/WO_3–SiO_2$. Metallic iridium is believed to be the active site for HC-SCR [23,24] and CO-SCR [15], and the reduction procedure is necessary for the formation of metallic iridium. Moreover, the reduction procedure markedly changed the oxidation state of tungsten, as shown by the XRD results. Although WO_3 is known to form alloys with various metals upon reduction [21] and an Ir–W alloy has been shown to have high resistance against oxidation [25], 600 °C is too low a temperature for the formation of an Ir–W alloy [26]. We observed only a small difference between the activities of the samples reduced at 400 °C to 600 °C, and we also confirmed that W metal and WO_2 were not observed by XRD after reduction at 400 °C. This result suggests that severe reduction to form W and WO_2 was not dispensable. H_2 consumption below 500 °C in H_2-TPR of $Ir/WO_3(10)–SiO_2$-2 was insufficient for the formation of WO_2. Therefore, we suggest that the necessary oxidation state of tungsten after reduction is WO_{3-x} ($0 < x < 1$).

We believe that the re-oxidation step was necessary for the formation of WO_3 with low reducibility as a support for iridium. Although the H_2-TPR profile of $Ir/WO_3–SiO_2$ after calcination showed a broad peak at 350 °C, the peak disappeared in the H_2-TPR profile of $Ir/WO_3–SiO_2$ after re-oxidation. H_2 consumption at around 200 °C in the H_2-TPR measurement of the re-oxidized sample was about 0.4 times the amount expected for stoichiometric IrO_2 reduction. These results suggest that the iridium particles were composed mainly of metallic iridium and that the reducibility of WO_3 was decreased by re-oxidation. Bigey et al. have reported that re-oxidized tungsten oxides exhibit lower reducibility than fresh WO_3 [21]. It is known that the oxidation state of tungsten is easily changed during reactions such as cracking and isomerization of hydrocarbons and that retaining a stable oxidation state of tungsten with high activity is difficult [20]. We suspect that the decrease in the reducibility of WO_3 was important for maintaining an active metallic iridium surface. It is concluded that the final active site formed by sequential treatments was metallic-state iridium finely dispersed on WO_3 having small particle size and resistance to reduction.

5. Conclusions

$Ir/WO_3–SiO_2$ showed high activity for selective NO reduction by CO. We attempted to optimize the conditions for preparation of the catalyst. The optimum composition was 0.5 wt% Ir and 1–30 wt% WO_3 in the support. At the optimum WO_3 contents, NO_x conversions were almost the same for all WO_3 contents. The surface area of $Ir/WO_3–SiO_2$ depended on SiO_2 content. Although the combination of WO_3 and SiO_2 as a support was effective for dispersing Ir/WO_3, the surface area did not influence the CO-SCR activity. The H_2-TPR results indicated that the catalysts with the optimum WO_3 content had lower reducibility of WO_3 than the catalysts with a high-WO_3 content.

Pretreatment after Ir loading (that is, calcination, reduction, and additional treatment) strongly influenced the CO-SCR activity. The optimum sequence of pretreatment was calcination in the presence of O_2 and H_2O followed by H_2 reduction and then re-oxidation under mild oxidizing conditions. TPD of nitrogen-containing compounds during calcination suggested that the NH_3 ligands in the Ir precursor were removed by oxidation in the presence of O_2 but that NH_3 release under a reducing condition occurred at a lower temperature than oxidative removal of the NH_3 ligands. H_2O addition lowered the temperature for oxidative removal of the NH_3 ligands. During the reduction, iridium was reduced to the metallic state, and WO_3 was also reduced to metal and WO_2. The reduction of WO_3 at least to WO_{3-x} ($0 < x < 1$) was required to activate the catalyst. H_2-TPR results suggested that re-oxidation suppressed the reducibility of WO_3. The re-oxidation step formed the favorable state of tungsten oxide as a support for iridium. XRD and TEM results suggested that very small WO_3 particles were dispersed on SiO_2. We concluded that the active state of the $Ir/WO_3–SiO_2$ catalysts, which was formed by sequential treatments, was metallic-state iridium finely dispersed on WO_3, which had small particle size and resistance to reduction.

References

[1] M. Iwamoto, H. Yahiro, S. Shundo, Y. Yu-u, N. Mizuno, Appl. Catal. 69 (1991) L15.
[2] W. Held, A. König, T. Richter, L. Puppe, SAE Tech. Pap. Ser. No. 900496 (1990).
[3] V.I. Pârvulescu, P. Grange, B. Delmon, Catal. Today 46 (1998) 233.
[4] A. Obuchi, A. Ohi, M. Nakamura, A. Ogata, K. Mizuno, H. Ohuchi, Appl. Catal. B 2 (1993) 71.
[5] R. Burch, T.C. Watling, J. Catal. 169 (1997) 45.
[6] J.L. d'Itri, W.M.H. Sachtler, Catal. Lett. 15 (1992) 289.
[7] S. Sato, Y. Yu-u, H. Yahiro, N. Mizuno, M. Iwamoto, Appl. Catal. 70 (1991) L1.
[8] H. Hamada, Y. Kintaichi, M. Inaba, M. Tabata, T. Yoshinari, H. Tsuchida, Catal. Today 29 (1996) 53.
[9] Y. Torikai, H. Yahiro, N. Mizuno, M. Iwamoto, Catal. Lett. 9 (1991) 91.
[10] D. Jun, K. Ishi, N. Iida, JSME Int. J. Ser. B 46 (2003) 60.
[11] J.T. Kummer, J. Phys. Chem. 90 (1986) 4747.
[12] M.L. Unland, J. Phys. Chem. 77 (1973) 1952.
[13] M.L. Unland, J. Catal. 31 (1973) 459.
[14] M. Ogura, A. Kawamura, M. Matsukata, E. Kikuchi, Chem. Lett. (2000) 146.
[15] M. Haneda, Pursparatu, Y. Kintaichi, I. Nakamura, M. Sasaki, T. Fujitani, H. Hamada, J. Catal. 229 (2005) 197.
[16] M. Shimokawabe, N. Umeda, Chem. Lett. 33 (2004) 534.
[17] M. Shimokawabe, M. Niitsu, H. Inomata, N. Iwasa, M. Arai, Chem. Lett. 34 (2005) 1426.
[18] T. Nanba, S. Shinohara, J. Uchisawa, S. Masukawa, A. Ohi, A. Obuchi, Chem. Lett. 35 (2006) 450.
[19] J. Oi, A. Kishimoto, T. Kudo, J. Solid State Chem. 103 (1993) 176.
[20] C. Bigey, L. Hilaire, G. Maire, J. Catal. 198 (2001) 208.
[21] C. Bigey, L. Hilaire, G. Maire, J. Catal. 184 (1999) 406.
[22] A. de Lucas, J.L. Valverde, P. CanÄizares, L. Rodriguez, Appl. Catal. A 172 (1998) 165.
[23] M. Nawdali, E. Iojoiu, P. Gélin, H. Praliaud, M. Primet, Appl. Catal. A 220 (2001) 129.
[24] C. Wögerbauer, M. Maciejewski, A. Baiker, J. Catal. 205 (2002) 157.
[25] Y. Abe, E. Watanabe, K. Sasaki, S. Iura, Surf. Coat. Technol. 198 (2005) 148.
[26] J.J. Kolodziej, T.E. Madey, Phys. Rev. B 62 (2000) 5150.